



Fluorescent cyclin-dependent kinase inhibitors block the proliferation of human breast cancer cells

Venkata Mahidhar Yenugonda^{a,b}, Tushar B. Deb^b, Scott C. Grindrod^{a,b}, Sivanesan Dakshanamurthy^{a,b}, Yonghong Yang^{a,b}, Mikell Paige^{a,b}, Milton L. Brown^{a,b,*}

^a Drug Discovery Program, Georgetown University Medical Center, 3970 Reservoir Rd, NW, Research Building, EP-07, Washington, DC 20057, USA

^b Department of Oncology, Lombardi Comprehensive Cancer Center, Georgetown University Medical Center, Research Building, Washington, DC 20057, USA

ARTICLE INFO

Article history:

Received 16 December 2010

Revised 24 February 2011

Accepted 28 February 2011

Available online 4 March 2011

Keywords:

Fluorescent
CDK inhibitors
Purvalanol B
Breast cancer
In vitro anti-cancer

ABSTRACT

Inhibitors of cyclin-dependent kinases (CDKs) are an emerging class of drugs for the treatment of cancers. CDK inhibitors are currently under evaluation in clinical trials as single agents and as sensitizers in combination with radiation therapy and chemotherapies. Drugs that target CDKs could have important inhibitory effects on cancer cell cycle progression, an extremely important mechanism in the control of cancer cell growth. Using rational drug design, we designed and synthesized fluorescent CDK inhibitors (**VMY-1-101** and **VMY-1-103**) based on a purvalanol B scaffold. The new agents demonstrated more potent CDK inhibitory activity, enhanced induction of G2/M arrest and modest apoptosis as compared to purvalanol B. Intracellular imaging of the CDK inhibitor distribution was performed to reveal drug retention in the cytoplasm of treated breast cancer cells. In human breast cancer tissue, the compounds demonstrated increased binding as compared to the fluorophore. The new fluorescent CDK inhibitors showed undiminished activity in multidrug resistance (MDR) positive breast cancer cells, indicating that they are not a substrate for p-glycoprotein. Fluorescent CDK inhibitors offer potential as novel theranostic agents, combining therapeutic and diagnostic properties in the same molecule.

© 2011 Elsevier Ltd. All rights reserved.

1. Introduction

Cyclin-dependent kinases (CDK) are classic Ser/Thr kinases with molecular weights of 30–40 kDa. This family of enzymes plays an important and well-defined role in cell cycle regulation and proliferation. CDK enzymatic activation requires the binding of specific regulatory subunits, termed cyclins, CDK-cyclin complexes are necessary for phosphorylation of key proteins that regulate the orderly progression through the cell cycle.^{1–4} Abnormal activation of various CDKs can ultimately lead to deregulated cell cycle progression, a common feature in many cancers.^{5,6} Given the pivotal role that dysregulation of CDK activity plays in cancers, targeting the CDKs is a viable strategy for blocking and/or interfering with tumor cell proliferation.^{7–9}

Thirteen CDK's and at least 29 cyclins have been discovered from the human genome¹⁰ and have been extensively characterized in regards to controlling cell cycle. Mutations in CDK proteins can result in the overexpression and altered function of CDK's and specific cyclins. In human tumors, mutations have been reported which result in the specific overexpression of cyclins D1 and E1 and CDK4 and CDK6.^{11,12}

Mutations in either CDK4 or cyclin D1 are implicated in primary solid tumors including breast, lung, pancreatic, gastrointestinal, head and neck, liver, and prostate. CDK6 is mutated in a smaller number of solid human cancers such as lymphomas, sarcomas and gliomas. CDK2 is rarely mutated in cancer. Aberrant activation of CDK1 has also been observed in a number of primary tumors including breast, colon, prostate, oral and lung.^{10,13}

Approximately 24 CDK inhibitors are currently in development or clinical trials. These molecules can be classified in at least four general categories including the purines, alkaloids, butyrolactones, and flavonoids.^{14–20} Despite differences in chemical structures, most CDK inhibitors competitively inhibit ATP binding at the catalytic site.^{21,22} The specificity of the inhibitors is a major concern due to a high degree of sequence similarity within the active site of the CDKs and a large number of other protein kinases. In addition, the ability to monitor intracellular delivery and intratumoral distribution remains difficult. Therefore, development of potent CDK inhibitors that provide an imageable 'readout' may be advantageous in the development of clinically effective therapeutic drugs.

The 2,6,9-trisubstituted purine analogs (olomoucine and roscovitine) and the purvalanols have been shown to selectively inhibit a subset of CDK's.¹⁵ These inhibitors act by selectively competing with ATP at its binding site in targeted CDK's, however purvalanol

* Corresponding author. Tel.: +1 202 687 8603; fax: +1 202 687 7659.

E-mail address: mb544@georgetown.edu (M.L. Brown).

B has been shown to target CDK2 and CDK1 complexes at submicromolar concentrations.¹⁶ Importantly, the carboxylic acid of the 6-anilino group of the purvalanol B (Fig. 1A) can be modified without negatively affecting their CDK-inhibitory activity,^{23,24} providing a strategy for the development of modified purvalanol B analogs.

Dansyl fluorochromes have been used in tracking small molecules intracellularly.^{25–28} By synthetically coupling the fluorescent compound dansyl-ethylenediamine to purvalanol B, two fluorescent analogs of purvalanol B, termed **VMY-1-103** and **VMY-1-101** were developed (Fig. 1B). These compounds were evaluated for their CDK inhibitory activity and for their in vitro effects in two human breast cancer cell lines (p53-mutated, estrogen-independent MDA-MB-231 cells and p53 wild type, estrogen dependent MCF-7 cells).

2. Results

2.1. Chemistry

The CDK2–purvalanol B crystal structure (PDB ID: 1CKP) revealed that the carboxylic acid of the 6-anilino substituent points outside of the ATP-binding pocket, and does not interfere with interior interactions of the kinase active site.^{13,27,28} Taking advantage of this structural arrangement, we synthetically coupled a fluorescent tag, dansyl ethylenediamine to the carboxylic acid of the 6-anilino substituent of purvalanol B. The newly synthesized fluorescent compounds **VMY-1-101** and **VMY-1-103** were prepared following a four-step synthetic route outlined in Figure 2A. Briefly, starting from commercially available 2-fluoro-6-chloropurine (**1**), standard regioselective N-9 alkylation with 2-propanol under Mitsunobu conditions gave 2-fluoro-6-chloro-9H-isopropylpurine. The 6-position was substituted with dansyl ethylenediamine, followed by substitution at the 2-position with (*R*)-2-amino-1-butanol to afford **VMY-1-101**, or (*R*)-valinol to give **VMY-1-103**.

2.2. Molecular modeling

To better understand the binding interactions between CDK2 and **VMY-1-103**, a structural model of the CDK2/**VMY-1-103** complex was developed (Fig. 2B). To provide consistent results, the docked position was remodeled by step-by-step manual docking with a restrained MD simulations followed by minimization. In the restrained MD simulations, the optimum Van der Waals and H-bond distance constraints were set between the ligand and the interacting residues.

The model suggests that the N7 imidazole nitrogen of the purine ring and the N6 amino group make a H-bond network with the backbone –NH and carbonyl of Leu83, respectively. The acidic C8 atom of the purine ring may form a weak H-bond with the carbonyl oxygen of Glu81. The C2 side chain of **VMY-1-103** is bound within the ATP ribose-binding pocket (Fig. 2A), with the isopropyl group interacting hydrophobically with the glycine-rich loop and Val18. The hydroxyl group of the *R* isopropyl group can make a H-bond with the backbone carbonyl of Gln131. The purine N9 isopropyl group shows a strong hydrophobic interaction with the hydrophobic side chains of Val18, Ala31, Phe80, Leu134, and Ala144. The chlorinated benzene ring of **VMY-1-103** shows a stacking interaction with Phe82, and a strong polar interaction between the Cl atom and the side chain of Asp86. Networks of H-bonds may be formed by the carbonyl and –NH group of the amide of **VMY-1-103**, the carbonyl can form a H-bond with Trp541 and the –NH can form a H-bond with Asp86. Furthermore, the sulfonamide group of the dansyl moiety can make a H-bond with Leu88, and the aryl component of dansyl group itself can make a hydrophobic contact with Leu89 and Asp92.

Upon overlay of purvalanol B with **VMY-1-103** (Fig. 2B), we noted that the both occupy a similar space in the binding pocket and form similar interactions. The only difference noted was that the –COOH group in purvalanol B, forms a H-bond with Trp541 and Leu89, whereas **VMY-1-103** cannot because of the steric constraints imposed by the amide group substituent. The increased affinity of **VMY-1-103** over purvalanol B can be rationalized from

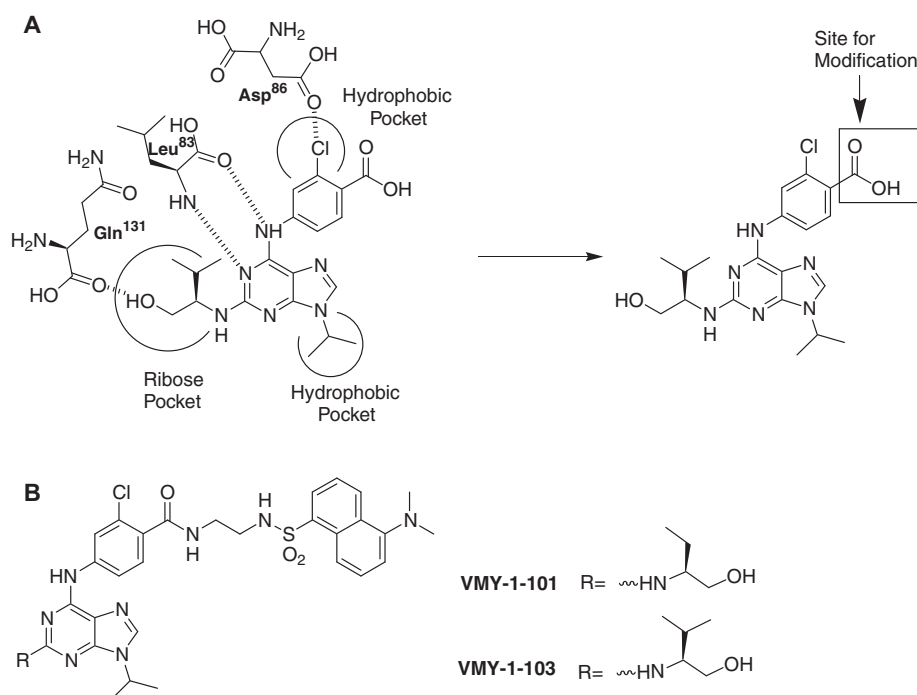


Figure 1. (A) Design strategy for a new class of fluorescent CDK molecules and (B) fluorescent purvalanol B analogues.

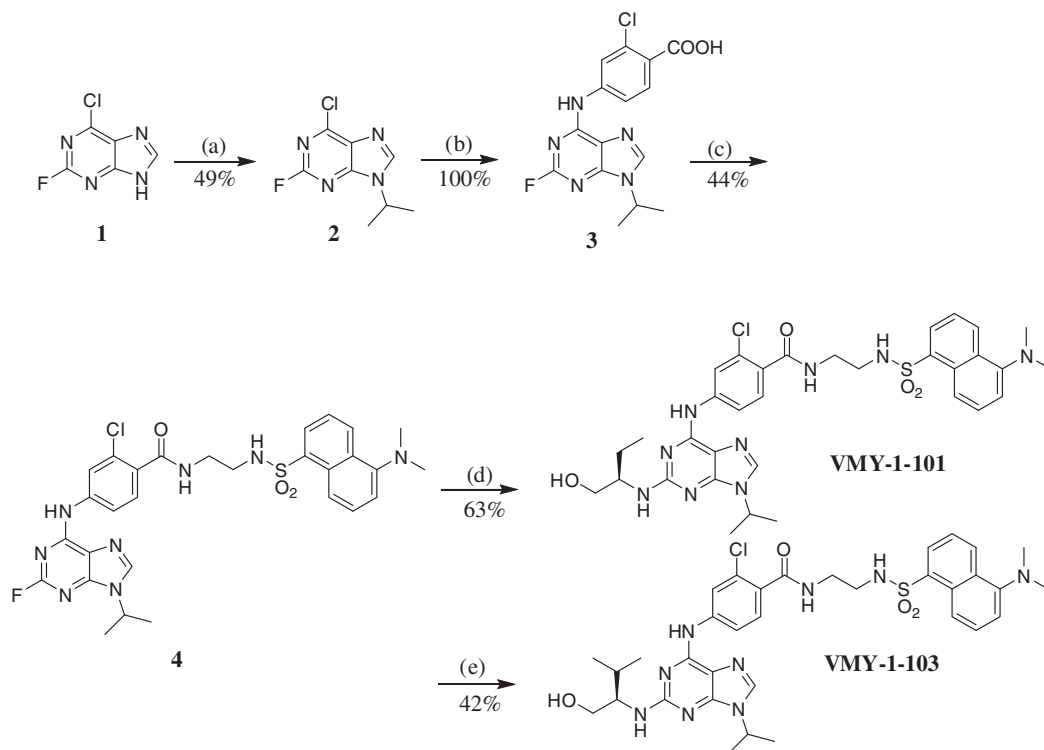


Figure 2A. Synthetic scheme. Reagents and conditions: (a) *i*PrOH, DEAD, PPh₃, THF, –10 °C–rt; (b) 4-amino-2-chloro-benzoic acid, DIEA, *n*-butanol, 80 °C; (c) Dansyl ethylenediamine, DIEA, EDCI, HOBT, DMF–CH₂Cl₂–dioxane (1:1:1); (d) (*R*)-2-amino-1-butanol (excess), DIEA, 120 °C, 48 h; (e) (*R*)-2-amino-3-methyl-1-butanol, DIEA, *n*-butanol, 120 °C, 72 h.

these binding interactions formed by the extended substituent at the N6-position of the benzene ring outside of the ATP-binding pocket.

3. Biological evaluation of compounds

3.1. Inhibition of Cdk isoforms activity by VMY-1-101 and VMY-1-103

The inhibitory activities of newly synthesized compounds were evaluated against several cell-free cyclin-dependent kinases. Interestingly, **VMY-1-101** and **VMY-1-103** were found to be potent competitive inhibitors of ATP as tested against various cell cycle kinases compared to roscovitine. In fact **VMY-1-101** and **VMY-1-103** showed a greater percent inhibition of CDK2/cyclin E complex as compared to other kinases (Table 1).

3.2. VMY-1-101 and VMY-1-103 compounds inhibit the in vitro growth of breast cancer cells or multidrug resistant cells

Based on the potency in the in vitro cell-free enzyme kinase assay, we further evaluated the anti-proliferative effects of our analogs on estrogen-independent (MDA-MB-231) and estrogen dependent (MCF-7) human breast cancer cell by WST-1 assay. The data (Table 2) indicate that the newly synthesized fluorescent compounds possess potent in vitro anti-proliferative activity (IC_{50} = 4.86–4.06 μ M or 10–19 μ M for **VMY-1-103** or **VMY-1-101**, respectively) independent of cell type. No significant anti-proliferative effects were observed for purvalanol B or dansyl ethylenediamine in either cell lines even at a concentration of 100 μ M.

Advanced stages of cancer often display resistance to anticancer drugs, this is considered one of the major obstacles to practical chemotherapeutic interventions. One mechanism of multidrug resistance (MDR) is the expression of a reflux pump (mediated

by P-glycoprotein-dependent or P-glycoprotein-independent mechanisms) that transports drugs out of the cells. In order to evaluate the MDR effect on **VMY-1-103**, we tested the effect of **VMY-1-103** on the proliferation in CL 10.3 (MDR-positive) cells, which over express P-glycoprotein,²⁹ and compare with MDR-negative MCF-7 cells. Paclitaxel, a known P-glycoprotein substrate³⁰ was included as a positive control. In Table 3, the IC_{50} of the compounds are represented along with the ratio of difference between MDR-positive and MDR-negative cell lines. In contrast to paclitaxel, **VMY-1-103** had comparable activity in both cell lines, and the activity did not seem to be modulated by MDR.

The anti-proliferative effects of **VMY-1-101** and **VMY-1-103** further correlate with morphological changes associated with cancer cells. As shown in Figure 3, a marked decrease in the cell number and aberrant gross morphological changes was observed in cells exposed to 10 μ M of the agent for 48 h. These results further confirm that the newly synthesized fluorescent compounds induce less density of cells by promoting induction of cell death.

3.3. Compounds (VMY-1-101 and VMY-1-103) induce cell cycle arrest at G2/M phase

To examine the relationship between growth inhibitory effect of the newly synthesized compounds and the expression of cell cycle proteins, we first analyzed the effects of the compounds on cell cycle distribution. Asynchronous breast cancer cells were treated for 16, 24 and 40 h with DMSO alone (control), 5 μ M, or 10 μ M of **VMY-1-101** or **VMY-1-103** or Roscovitine and purvalanol B. Figure 4A are representative cell cycle histograms for 24 h time intervals. Results shows with the percentage of cells in each phase after subtracted from untreated cells. After treatment with compounds, a clear accumulation of cells in the G2-M phase was detected irrespective of origin of the cell lines. There was also a moderate increase in cells containing sub-G1 amount of DNA indicating that the present fluorescent compounds were inducing cell death. Sim-

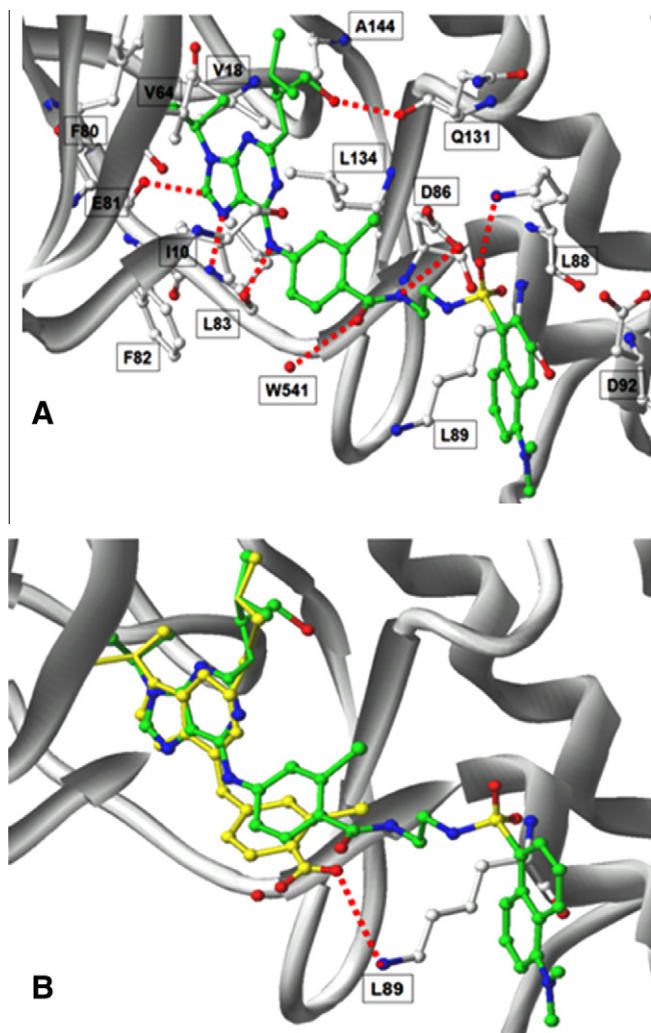


Figure 2B. VMY-1-103 modeled in the ATP-binding pocket of CDK2 (A): H-bond interactions are indicating by dotted lines (red) connecting the respective residues. CDK2 is represented by ribbon model and residues interacting with VMY-1-103 shown by ball and stick model. VMY-1-103 is shown in a stick representation with its carbon atoms colored in green. (B) Overlay of VMY-1-103 with purvalanol B (yellow).

ilar patterns of G2/M phase arrest were observed at 16- and 40-h time intervals (data not shown).

3.4. Reversible/irreversible effect of VMY-1-103 on breast cancer cell proliferation

In order to examine the reversible/irreversible mechanism of the anti-proliferative effect of the fluorescent compounds, we exposed MDA-MB-231 cells to 5 μ M or 10 μ M of VMY-1-103 for

Table 1
Inhibitory effects of VMY-1-101 and VMY-1-103 on CDK's activity

Protein kinase	VMY-1-101 (0.1 μ M)	VMY-1-103 (0.1 μ M)	R-Roscovitine (0.1 μ M)	Purvalanol B (0.1 μ M)
CDK1/cyclin B	16 \pm 3	35 \pm 1	10 \pm 5	78 \pm 6
CDK2/cyclin A	62 \pm 0	72 \pm 1	41 \pm 4	96 \pm 0
CDK2/cyclin E	87 \pm 0	89 \pm 1	57 \pm 4	98 \pm 0
CDK3/cyclin E	40 \pm 3	65 \pm 3	20 \pm 7	89 \pm 0
CDK5/p25	76 \pm 1	75 \pm 5	40 \pm 1	97 \pm 0
CDK5/p35	67 \pm 1	66 \pm 5	41 \pm 1	97 \pm 0
CDK7/cyclin H/MAT1	57 \pm 0	69 \pm 2	26 \pm 5	66 \pm 1
CDK9/cyclin T1	44 \pm 1	67 \pm 3	19 \pm 1	22 \pm 0

Note: CDK, cyclin-dependant kinase. The inhibitor concentrations are shown in parenthesis. Kinase inhibition represented as a percentage of control ($N=2$) with \pm SD. Compounds were tested at 100 nM concentrations on 8 purified kinases as described in Section 5.1.

Table 2

Effects of VMY-1-101 and VMY-1-103 on the survival of human breast cancer cell lines

Cell survival (WST-1 reduction, IC ₅₀ , μ M, 48 h)		
Compound	MDA-MB-231 (ER-)	MCF-7 (ER+)
VMY-1-101	4.86 \pm 1.24	19.05 \pm 1.14
VMY-1-103	4.06 \pm 1.32	10.03 \pm 1.25
R-Roscovitine	54.64 \pm 1.27	55.01 \pm 1.1
Purvalanol B	>100	>100
Dansyl ethylenediamine	>100	>100

Note: VMY-1-101 and VMY-1-103 and controls were tested at various concentrations for effects on cell survival of breast cancer. Cell survival was estimated 48 h after the addition of each compound using the WST-1 reduction assay. Results shown are mean values of triplicate experiments. The IC₅₀ value (the concentration yielding 50% growth inhibition) was interpolated from the graph of the log of compound concentration versus the fraction of surviving cells. The IC₅₀ was calculated using graph pad prism. Data are expressed as mean (SEM) of triplicate experiments.

24 h. Further exposure to drug free media for additional 48 h. As shown in Figure 4B, VMY-1-103 induced cell cycle arrest at G2/M phase for 24 h and remains at G2/M phase after 48 h with drug free medium. In contrast, the control roscovitine induces the G2/M phase arrest at 24 h and returns to normal stage after 48 h with drug free medium. These results further indicate that the anti-proliferative effect of VMY-1-103 is irreversible.

3.5. Anti-proliferative mechanism of VMY-1-103

We evaluated purvalanol B and VMY-1-103 for their effects on G2/M cell cycle proteins. MDA-MB-231 cells were treated with purvalanol B and VMY-1-103 at 10 μ M and a comparison of cell cycle proteins expression at different time points were evaluated by western blotting. We specifically assessed the expression levels of principal component proteins for G2/M checkpoint, such as phospho-cdc2, cdc2, and cyclin B. As shown in Figure 5, after 6 h treatment, the VMY-1-103 treated cells resulted in a time-dependent decrease in expression of phospho-cdc2 at both the catalytic (T161) and regulatory (Y15) sites compared to control. Purvalanol B had no affect on the phospho-cdc2 expression throughout the time period tested. The inhibition of the expression level of phospho-cdc2 in MDA-MB-231 cells further supports that VMY-1-103 decreases the cdc2 (CDK1) kinase activity, which halts cell division at the G2/M check point. Quantitative analysis of these bands showed a statistically significant difference between VMY-1-103 and purvalanol B in terms of phospho expression levels of cdc2.

3.6. Intracellular localization of VMY-1-103

Activation of CDK1/cyclin B kinase activation is responsible for driving the G2/M phase of the cell cycle in the cytoplasm as the cells progress into metaphase.³¹ Taking advantage of the inherent fluorescent property of VMY-1-103, we examined the intracellular

Table 3
Effects of **VMY-1-103** and paclitaxel on the survival of multidrug resistant breast cancer cell lines

Cell line	Origin	Cell survival (WST-1 reduction, IC ₅₀ , μM, 72 h)	
		VMY-1-103	Paclitaxel
MCF-7	Breast	4.5 ± 1.19	0.002 ± 1.12
CL 10.3	Breast (MDR)	44.1 ± 1.18	>50
MDR IC ₅₀ /non-MDR IC ₅₀		9.8	>25,000

Note: **VMY-1-103** was tested at various concentrations for effects on cell survival of MDR cell line. Cell survival was estimated 72 h after the addition of each compound using the WST-1 reduction assay. Results shown are mean values of triplicate experiments. The IC₅₀ value (the concentration yielding 50% growth inhibition) was interpolated from the graph of the log of compound concentration versus the fraction of surviving cells. The IC₅₀ was calculated using graph pad prism. Data are expressed as mean (SEM) of triplicate experiments.

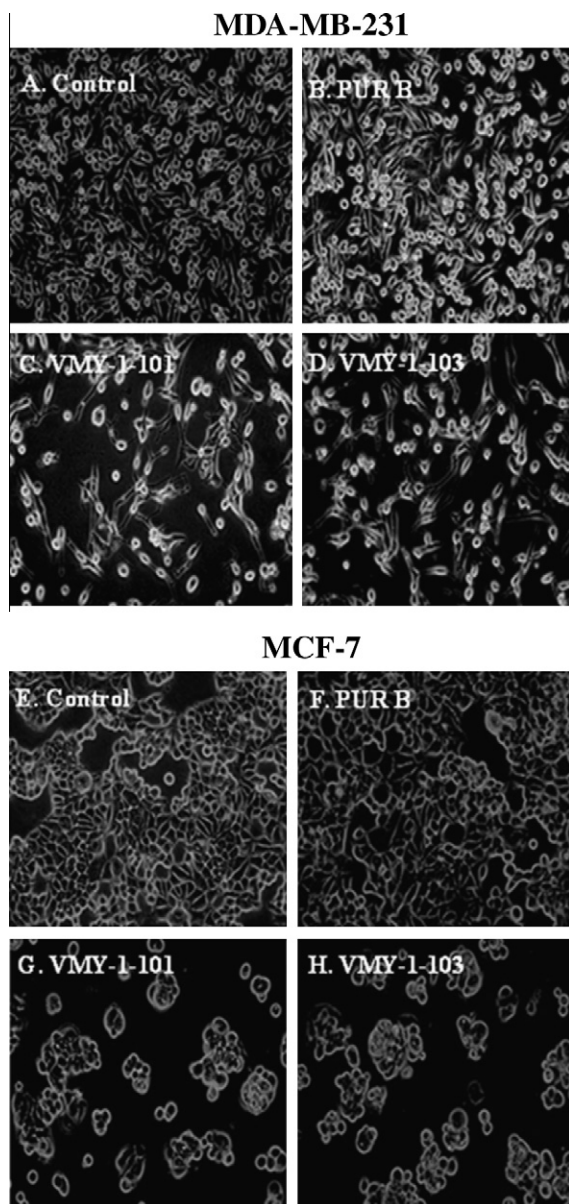


Figure 3. Morphological changes in human breast cancer cell lines after exposure to different compounds. MDA-MB-231 (A–D) and MCF-7 (E–H) were treated with 10 μM of purvalanol B, **VMY-1-101** and **VMY-1-103** for 48 h. After treatment, media was removed and washed with PBS. The images were captured with an olympus X71 inverted digital microscope system with a 20× bright field.

localization of **VMY-1-103** in breast cancer cells. Cells were treated with 10 μM of **VMY-1-103** for 1 h followed by fixation and visualization of cells by two-photon confocal microscopy. Propidium i-

did staining (red) was used to visualize the nucleus (Fig. 6B), and differential interference contrast (DIC) was used to reveal the morphology of the cells. In both cell lines (MDA-MB-231 and MCF-7), **VMY-1-103** localized into the cytoplasm. Similar results were also found at different time intervals such as 3, 6, 12, and 24 h (data not shown). The data supports our hypothesis that **VMY-1-103** binds to the inactive form of cdc2, which resides in the cytoplasm.

3.7. Binding of **VMY-1-103** to human breast cancer tissue

We evaluated the binding ability of **VMY-1-103** as compared to dansyl ethylenediamine (fluorophore alone) on human breast cancer tissue (Georgetown University tissue bank). Tissues were treated with a 10 μM solution of **VMY-1-103** or dansyl ethylenediamine and imaged by two-photon confocal microscopy. As shown in Figure 6C, **VMY-1-103** has strong binding affinity to binding to breast tissues as compared to the fluorophore alone. These results support binding of **VMY-1-103** and not chromophore fragment to the tissue, which is tethered on the solvent-exposed region of the **VMY-1-103**.

3.8. Apoptotic signaling

In order to understand whether the fluorescent compounds were able to induce apoptotic cell death, we evaluated the expression of anti and pro-apoptotic proteins in MDA-MB-231 cells after treatment with a 10 μM solution of each compound for 48 h. Western blot analysis of regulatory anti-apoptotic Bcl2 and pro-apoptotic Bax proteins for intrinsic apoptosis are shown in Figure 7A. These data indicate that the decreased level of anti-apoptotic proteins and increased level of pro-apoptotic protein for cells treated with **VMY-1-101** and **VMY-1-103** could upset the balance of pro- and anti-apoptotic proteins towards the expression of proteins favoring apoptosis. This was confirmed with cleaved of pro-apoptotic 116 kDa poly (ADP-ribose) polymerase protein (PARP) into its 89-kDa fragments. As shown in Figure 7B **VMY-1-101** and **VMY-1-103** promote moderate cleavage of the 116-kDa full length PARP into an 89-kDa fragment, a mechanism known to impair genomic integrity before apoptosis. We also observed decreased protein level of full length caspase 3 and 7 in cells treated with **VMY-1-101** and **VMY-1-103** (data not shown). Interestingly, there was no change in protein levels in roscovitine treated cells even at 40 μM. This further supports the hypothesis that, in contrast to roscovitine the present fluorescent compounds induce apoptosis mediated cell death in MDA-MB-231.

To investigate the programmed cell death (apoptosis) in MCF-7 cells (caspase-3 negative), we performed a biparametric cytofluorimetric analysis, using propidium iodide (PI) and annexin V-fluorescein isothiocyanate (FITC) which stain DNA and phosphatidylserine (PS) residues. Because externalization of PS occurs in the first stages of apoptosis, annexin-V staining identifies apoptosis at an earlier stage than sub-G1 appearance. After 24 h treatment of the compounds, MCF-7 cells were labeled with the two dyes and mon-

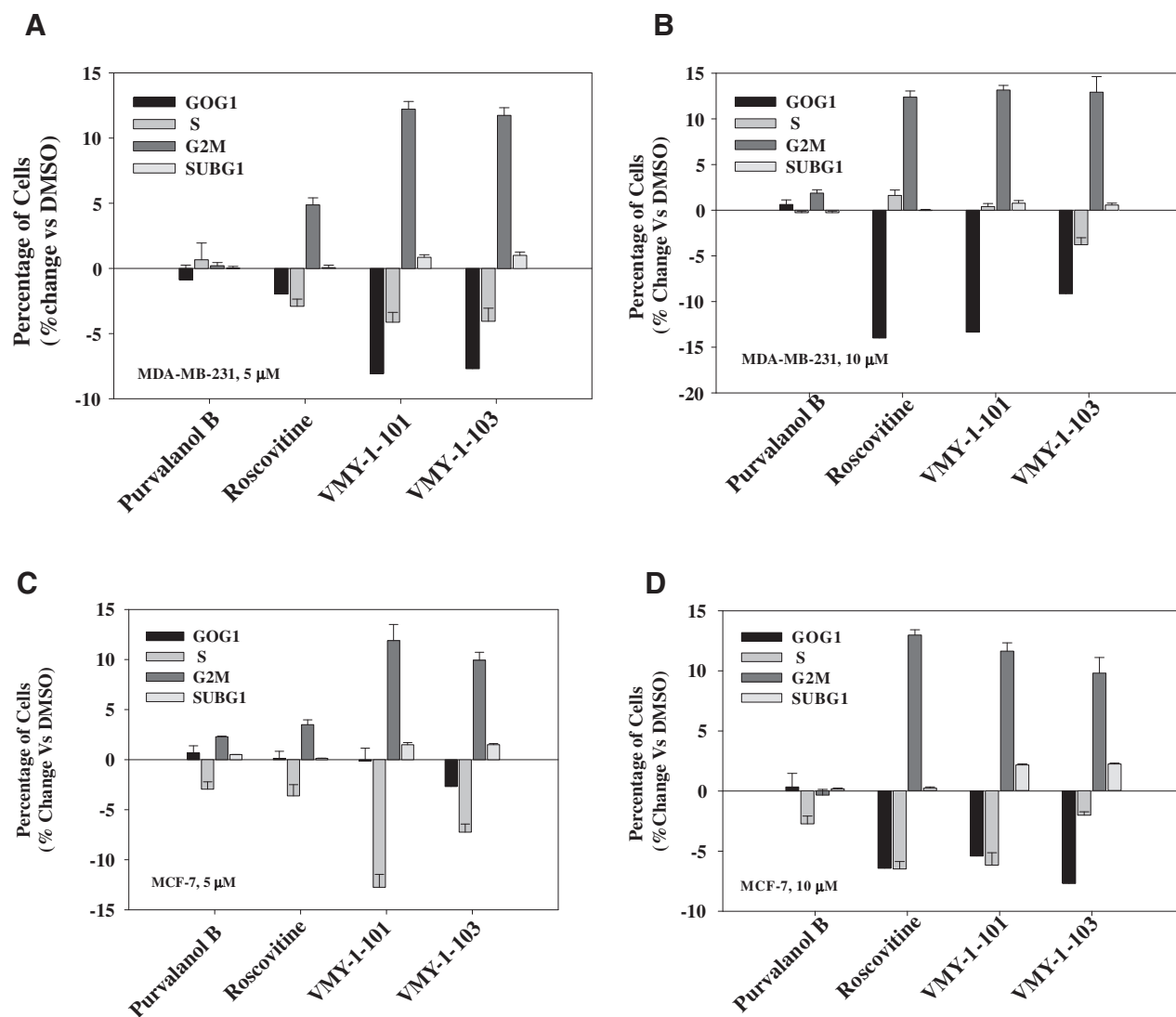


Figure 4A. Effect of compounds on cell cycle distribution. Asynchronised MDA-MB-231 cells were treated with 5 μ M (A) and 10 μ M (B) for 24 h and similarly asynchronised MCF-7 cells were treated with 5 μ M (C) and 10 μ M (D) for 24 h. Cell cycle distributions were determined by flow cytometry using propidium iodide staining of fixed cells (details as described in Section 5). The percentage of cells in each phase of the cell cycle is represented in the graph as subtracted values from DMSO treated cells (control). Results are represented as a mean of triplicate experiment.

itored by flow cytometry. As shown in Figure 7C, the newly synthesized fluorescent compounds provoked a significant induction of apoptotic cells in both early and late apoptotic cell population after 24 h treatment at 10 μ M. These findings further support the hypothesis that the fluorescent compounds induced apoptotic cell death in MCF-7 cells.

4. Discussion

Aberrant expression and activation of cell cycle regulatory proteins is a common feature of many cancers. Components of the cell cycle machinery, such as the CDKs, may therefore represent excellent molecular targets for the design of anticancer agents.³² Several classes of CDK inhibitors, including both natural³³ and chemically synthesized agents^{11,12} have been reported and several are in clinical trials.³² However as because the target specificity of CDK inhibitors is challenging, and in the absence of an efficient method of determining real time pharmacodynamics, there is a need to develop trackable, selective and potent CDK inhibitors.

The strategy described herein involved the use of the fluorescent property of a dansyl moiety in our compound design. We chemically modified purvalanol B (a potent CDK inhibitor) at the solvent exposed carboxylic acid region. Evaluation of the fluorescent compounds for inhibition of CDKs resulted in the discovery of two novel potent fluorescent CDK inhibitors (Fig. 1). **VMY-1-101** and **VMY-1-103** fluoresced with an excitation of 410 nm and emission of 512 nm (Fig. 6A). As shown in Table 1, **VMY-1-101** and **VMY-1-103** showed the greatest activity against CDK2/cyclin E (87% and 89% at 100 nM, respectively). The compounds were also found to be effective in inhibiting other CDKs, such as CDK1/cyclinB, and to have strong anti-proliferative activity against two human adenocarcinoma cell lines (p53-mutated, estrogen-independent MDA-MB-231 cells, and wild type p53, estrogen dependent MCF-7 cells) in vitro. The potent anti-proliferative activity of fluorescent compounds (**VMY-1-103** and **VMY-1-101**) were observed in two breast cancer cell lines (IC₅₀ 4.0–4.8 μ M in MDA-MB-231 cells and 10.0–19.0 μ M in MCF-7 cells), and was 13-fold more potent in inhibiting MDA-MB-231 cell growth and 2.8–5.5-fold more potent in inhibiting MCF-7 cell growth as compared to roscovitine.

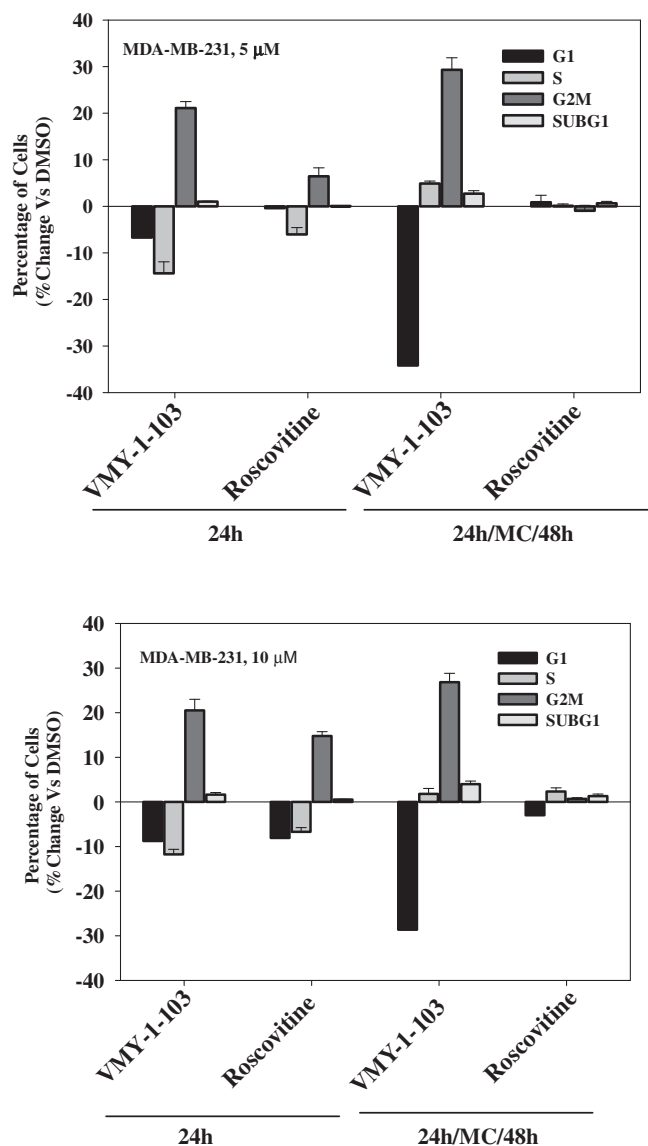


Figure 4B. Anti-proliferative effect of **VMY-1-103** is irreversible/reversible. Exponentially growing MDA-MB-231 cells were treated with **VMY-1-103** at 5 μ M (A) and 10 μ M (B). Cells were treated for 24 h and additionally, after post-incubation for 48 h in a compound free media (24 h/MC/48 h). Cell cycle distributions were determined by flow cytometry using propidium iodide staining of fixed cells (details as described in Section 5). The percentage of cells in each phase of cell cycle represented in the graph as subtracted values from untreated cells (control). Results are represented as a mean of triplicate experiments.

Interestingly, no anti-proliferative activity was found in these cell lines even at 100 μ M (Table 2). Morphological changes (Fig. 3) were induced by compounds **VMY-1-101** and **VMY-1-103** in both cell lines. Treatment of breast cancer cells with our compounds induced G2/M cell cycle arrest, independent of the estrogen status of the cells (Fig. 4A). Interestingly, in contrast to roscovitine, **VMY-1-103** showed irreversible anti-proliferative effects (Fig. 4B). **VMY-1-103** was also moderately active at inhibiting a multidrug resistance (MDR) positive cell line and we show that our analogs are not substrates for p-glycoprotein (Table 3).

Inhibition of the levels of phospho-cdc2 in MDA-MB-231 (Fig. 5), further support the hypothesis that **VMY-1-103** decreases the cdc2 kinase activity, and may play a central role in halting cell division in G2/M. Purvalanol B does not show any effect on levels of phospho-cdc2 in cellular assays, although it demonstrated more potent CDK1-inhibitory activity in the in vitro kinase assay than **VMY-1-**

103 (Table 1). This suggests that purvalanol B has poor cell penetration. Confocal imaging of treated cells confirmed the intracellular delivery of **VMY-1-103**, which localized in the cytoplasm of human breast cancer cells (Fig. 6B). The lipophilic dansyl ethylenediamine group may provide increased cell membrane permeability, enhancing intracellular delivery and concentration of **VMY-1-103**.⁴²

Treatment of cancer cells with the fluorescent CDK inhibitors resulted in the modulation of several key apoptotic and cell survival proteins, mediating apoptosis by down-regulating the anti-apoptotic protein Bcl-2, and inducing the pro-apoptotic protein, Bax (Fig. 7A). Induction of apoptosis was further confirmed by increased PARP cleavage in MDA-MB-231 cells (Fig. 7B) and increased annexin-V positivity in MCF-7 cells (Fig. 7C).

In summary, we have designed and synthesized a new class of fluorescent CDK inhibitors that are irreversible agents with potent anti-proliferative and pro-apoptotic capabilities in human breast cancer cell lines beyond that seen with the parent compound. These new CDK analogs also allowed for the visualization of their delivery to the cytoplasm of human breast cancer cells and tissues, and therefore provide a platform for future preclinical studies.

5. Experimental section

5.1. Materials

All reagents and solvents were commercially available and used without further purification. Chromatography was performed for purification of final compounds using a Biotage SP-1 system with silica gel cartridges. NMR spectra were recorded on a Varian 400 MR spectrometer at 400 MHz for H-1 and 100 MHz for C-13. Chemical shifts (δ) are given in ppm downfield from tetramethylsilane, and coupling constants (J -values) are provided in hertz (Hz). The purity of final compounds was evaluated by reverse-phase HPLC analysis (Shimadzu Model LC 2010) using two conditions as follows A = water, B = acetonitrile, method 1: 2–60% B in A over 20 min, method 2: 50–60% B in A over 20 min (Restek Ultra IBD 5 μ m column (4.6 mm \times 50 mm) at a flow rate of 1 mL/min).

5.2. Chemical synthesis

5.2.1. 6-Chloro-2-fluoro-9-isopropyl-9H-purine (2)

6-Chloro-2-fluoro-9H-purine (**1**) (1.8 g, 10.4 mmol) and triphenylphosphine (6 g, 20.8 mmol) in 60 mL of anhydrous tetrahydrofuran was added to a flame-dried flask under N₂. Anhydrous 2-propanol (1.6 mL, 20.8 mmol) was added and the mixture was cooled to –10 °C. After dropwise addition of 40% (w/v) diethyl azodicarboxylate in toluene (9 mL, 20.8 mmol), the mixture was warmed gradually to room temperature. After 18 h, the reaction mixture was quenched with 1 mL of water and the solvent was removed under reduced pressure. The resulting yellow oil was purified by column chromatography and the solid was triturated with methanol (to remove the diethyl hydrazine-*N,N'*-dicarboxylate ester by-product) to yield 1.1 g (49%) of a white solid.

¹H NMR (400 MHz, CDCl₃): δ 1.65 (d, 6H), 4.85 (m, 1H), 8.16 (s, 1H).

5.2.2. 2-Chloro-4-(2-fluoro-9-isopropyl-9H-purin-6-ylamino)benzoic acid (3)

4-Amino-2-chlorobenzoic acid (0.32 g, 1.9 mmol), 2-fluoro-6-chloro-9H-isopropylpurine (**2**) (0.4 g, 1.9 mmol), and diisopropylethylamine (0.8 mL, 2.5 mmol) were combined with *n*-butanol in a sealed tube and heated for 12 h at 80 °C. After removal of the solvent under reduced pressure, the crude product was triturated with CH₂Cl₂, the precipitate was collected by filtration, and washed with 0.05 M cold HCl (10 mL), CH₂Cl₂ (20 mL), and ether (20 mL) to

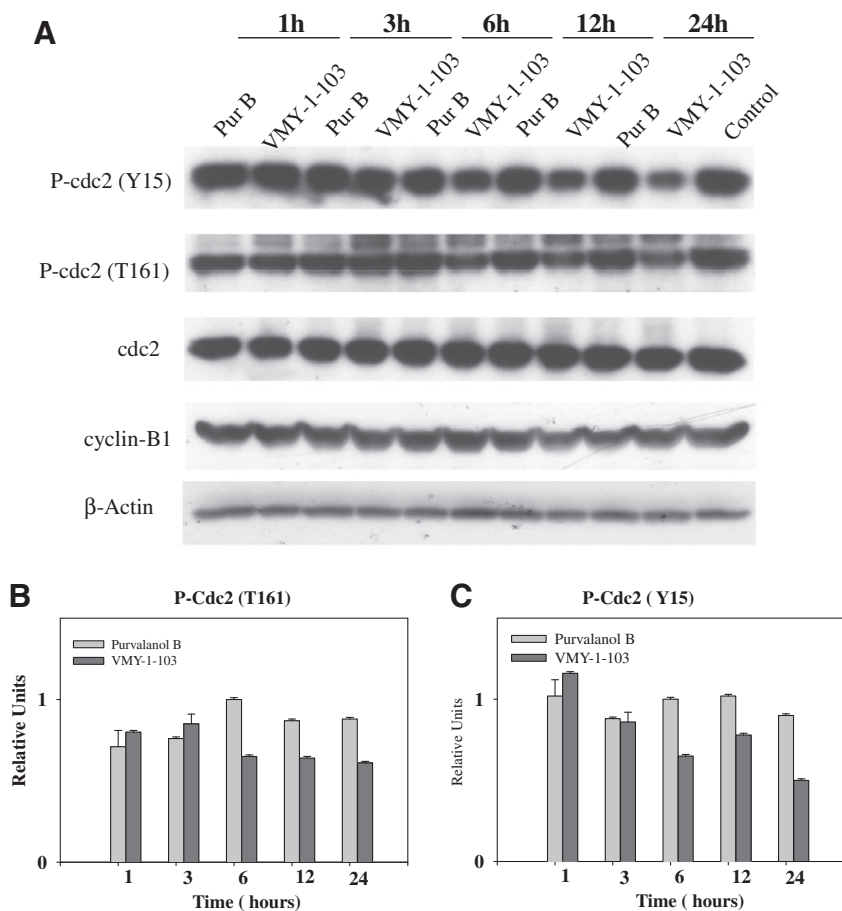


Figure 5. Mechanism of in vitro action of **VMY-1-103**. MDA-MB-231 cells treated with 10 μ M of purvalanol B and **VMY-1-103** at different time intervals (1, 3, 6, 12 and 24 h) and was subjected to western blot analysis to analyze the phosphorylation status of cdc2 substrates. Actin in each sample was employed as a standard. Below (B and C) are shown the quantification of bands of phospho-CDC2 (Y15), phospho-CDC2 (Y15), which were performed using NIH image analysis normalized to actin. Data are expressed as mean \pm SD for three values.

yield **3** as a white solid (0.68 g, 100%). The crude product was used without purification.

^1H NMR (400 MHz, $\text{DMSO}-d_6$): δ 1.51 (d, 6H, $J = 6.8$ Hz), 4.69 (m, 1H), 7.83 (d, 1H, $J = 8.7$ Hz), 7.93 (dd, 1H, $J = 2.1$ Hz, $J = 8.7$ Hz), 8.16 (d, 1H, $J = 2.0$ Hz), 8.46 (s, 1H), 10.74 (s, 1H).

5.2.3. 2-Chloro-*N*-(2-(5-(dimethylamino)naphthalene-1-sulfonamido)ethyl)-4-(2-fluoro-9-isopropyl-9H-purin-6-ylamino)benzamide (**4**)

Compound (**3**) (0.67 g, 1.9 mmol) and dansyl ethylenediamine³⁴ (0.74 g, 2.5 mmol) were dissolved in 30 mL of CH_2Cl_2 -dioxane-DMF (1:1:1 solution) and the resulting solution was added to a mixture of diisopropylethylamine (0.70 mL, 4.1 mmol) and HOBt hydrate (0.33 g, 2.5 mmol) followed by addition of EDCI (0.48 g, 2.5 mmol). The mixture was stirred for 24 h and then concentrated under reduced pressure. The residue was dissolved in chloroform (100 mL) and washed with 10% citric acid (30 mL), saturated LiCl solution and brine. The organic phase was separated, dried over anhydrous sodium sulfate, filtered, and concentrated under reduced pressure to give the crude product. The crude product was purified by column chromatography yielding 0.52 g (44%) of compound **4** as a yellow amorphous sticky solid. HRMS ($[\text{M}+\text{H}]$) calcd, 625.1912; found, 625.1724.

^1H NMR (400 MHz, CDCl_3): δ 1.58 (d, 6H, $J = 6.7$ Hz), 2.83 (s, 6H), 3.18 (dd, 2H, $J = 5.7$ Hz, $J = 10.8$ Hz), 3.49 (m, 2H), 4.75 (m, 1H), 6.95 (d, 2H, $J = 5.6$ Hz), 7.08 (d, 1H, $J = 7.6$ Hz), 7.34 (m, 2H), 7.47 (t, 1H, $J = 7.9$ Hz), 7.56 (dd, 1H, $J = 1.5$ Hz, $J = 8.6$ Hz), 7.87 (s, 1H), 7.94 (s, 1H), 8.25 (m, 2H), 8.49 (d, 1H, $J = 8.6$ Hz), 8.65 (s, 1H).

^{13}C NMR (100 MHz, CDCl_3) δ 166.9, 157.1, 152.8, 152.6, 151.9, 150.9, 150.8, 140.9, 139.4, 134.5, 131.2, 130.5, 129.783, 129.5, 129.4, 128.6, 128.3, 123.1, 120.9, 118.9, 118, 115.1, 47.7, 45.3, 42.9, 39.8, 22.4.

5.2.4. (*R*)-2-Chloro-*N*-(2-(5-(dimethylamino)naphthalene-1-sulfonamido)ethyl)-4-(2-(1-hydroxybutan-2-ylamino)-9-isopropyl-9H-purin-6-ylamino)benzamide (**VMY-1-101**)

A mixture of compound (**4**) (0.1 g, 0.16 mmol), (*R*)-(-)-2-amino-1-butanol (5 mL, 53 mmol), and diisopropylethylamine (0.2 mL, 1.21 mmol) was placed in a sealed tube and heated at 120 $^\circ\text{C}$ for 48 h. After cooling to room temperature, the reaction mixture was diluted with chloroform (100 mL), and washed with water and brine. The organic phase was separated and dried over anhydrous sodium sulfate, filtered, and concentrated under reduced pressure to give the crude product. The product was purified by flash chromatography to yield a pure amorphous sticky solid of **VMY-1-101** (0.070 g, 63%). HRMS ($[\text{M}+\text{H}]$) calcd, 694.2691; found, 694.2437.

^1H NMR (400 MHz): 0.98 (t, 3H, $J = 7.4$ Hz), 1.44 (dd, 6H, $J = 5.7$ Hz, $J = 20.9$ Hz), 1.62 (m, 2H), 2.84 (s, 6H), 3.18 (brs, 2H), 3.49 (tt, 2H, $J = 7.1$ Hz, $J = 19.7$ Hz), 3.65 (m, 1H), 3.91–4.03 (m, 2H), 4.47 (s, 1H), 5.43 (d, 2H), 7.10 (dd, 2H, $J = 2.7$ Hz, $J = 7.9$ Hz), 7.45 (m, 4H), 7.57 (s, 1H), 7.86 (s, 1H), 8.23 (dd, 1H, $J = 1.1$ Hz, $J = 7.3$ Hz), 8.34 (d, 1H, $J = 8.6$ Hz), 8.50–8.55 (m, 1H).

^{13}C NMR (100 MHz, CDCl_3): δ 167.1, 159.2, 151.8, 151.3, 151.1, 142.0, 135.4, 134.9, 130.8, 130.3, 129.8, 129.5, 129.3, 128.2, 127.2,

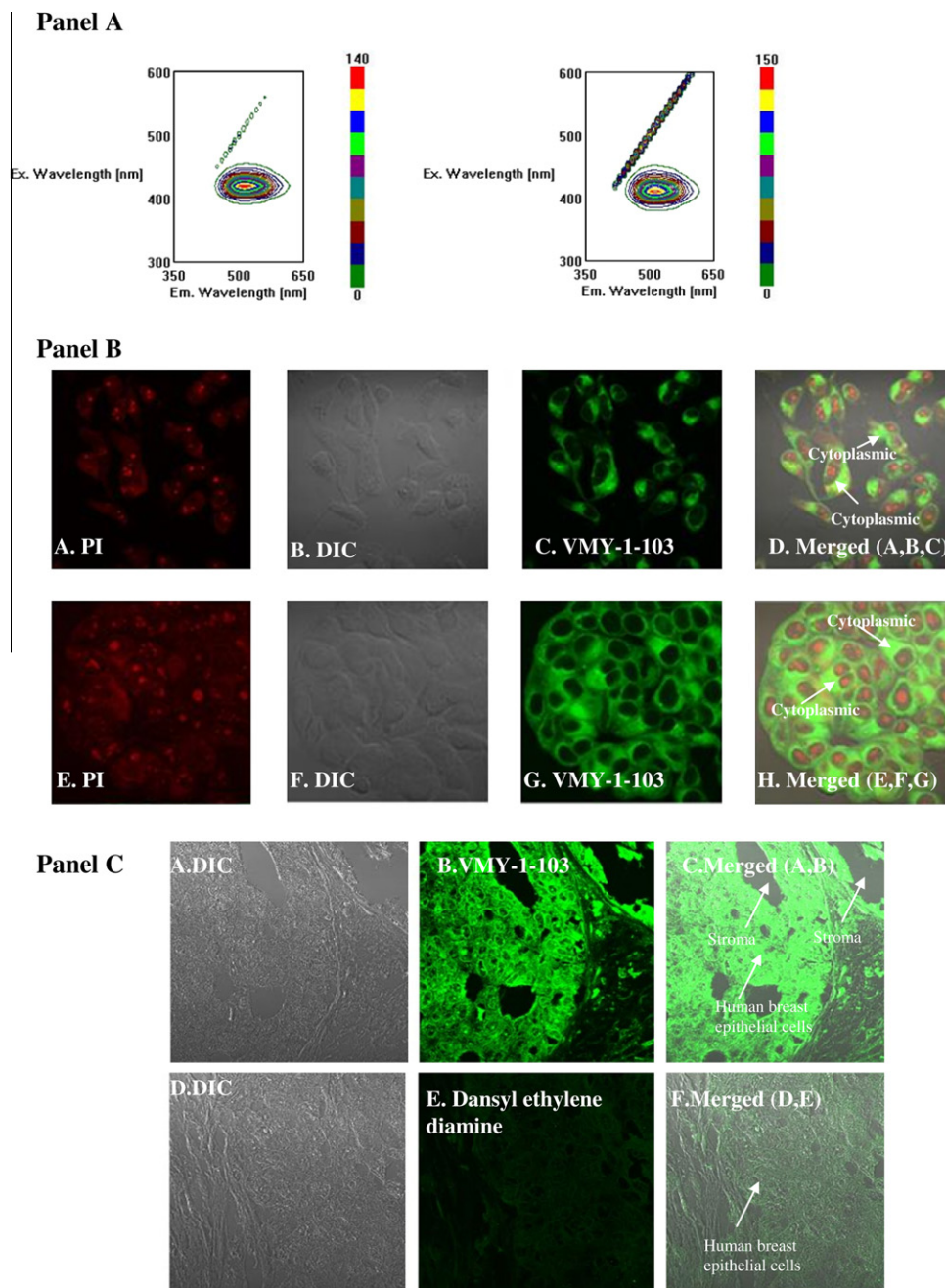


Figure 6. Panel A: Fluorescence spectrum of dansyl ethylenediamine (left, excitation/emission, 410/512 nm) and **VMY-1-103** (right, excitation/emission, 410/512 nm). Both compounds were dissolved in methanol and fluorescence spectrums were measured by fluorescent spectrophotometer. Panel B: Confocal images of MDA-MB-231 (A–D) and MCF-7 (E–H) of human breast cancer cell lines treated with **VMY-1-103**. Cells (5×10^5) were treated with the 10 μM **VMY-1-103** for 1 h. After treatment, cells were washed with PBS, fixed with 4% formaldehyde in PBS, stained with PI, and mounted on glass slides. The Zeiss LSM510/META/NLO live imaging multiphoton microscope was used to visualize the fluorescence with 63 \times magnification. Excitation was at 720 nm and absorbance was read at bandpath filter of 480–520 nm. Panel C: Binding of **VMY-1-103** in human breast tissues. After epitope retrieval of human breast cancer tissue as described in Section 5.1, exposed to 10 μM **VMY-1-103** and dansyl ethylenediamine (control) for 1 h. After treatment, tissues were washed with water, mounted with aqua mount. Zeiss LSM510/META/NLO live imaging multiphoton microscope was used to visualize the fluorescence with magnification $\times 63$. Excitation was at 720 nm and absorbance was read at bandpath filter of 480–520 nm.

123.1, 120.0, 118.8, 117.2, 115.1, 114.5, 65.3, 55.5, 53.4, 46.5, 45.3, 42.7, 40.2, 24.8, 22.5, 22.3, 10.7.

5.2.5. (R)-2-Chloro-N-(2-(5-(dimethylamino)naphthalene-1-sulfonamido)ethyl)-4-(2-(1-hydroxy-3-methylbutan-2-ylamino)-9-isopropyl-9H-purin-6-ylamino)benzamide (**VMY-1-103**)

Compound (**4**) (0.15 g, 0.24 mmol), (R)-(-)-2-amino-3-methyl-1-butanol (0.12 g, 1.2 mmol), and diisopropylethylamine (0.2 mL,

1.2 mmol) were dissolved in *n*-butanol in a sealed tube and heated to 120 $^{\circ}\text{C}$ for 24 h. After 24 h, (R)-(-)-2-amino-3-methyl-1-butanol (0.04 g, 0.38 mmol) and 0.2 mL (1.2 mmol) of diisopropylethylamine were added and the reaction was allowed to stir for 48 h. After removal of the solvent under reduced pressure, the crude product was dissolved in CH_2Cl_2 , and washed with water (50 mL) followed by brine (50 mL). The organic phase was separated and dried over anhydrous sodium sulfate, filtered, and concentrated under reduced pressure to give 0.1 g of crude

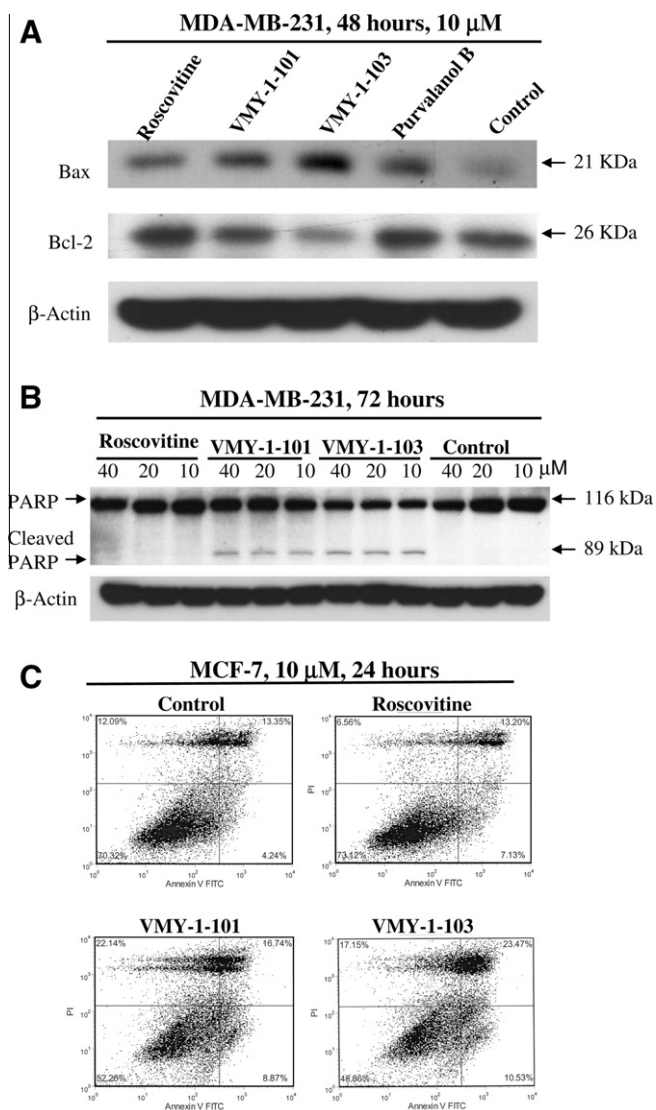


Figure 7. Effects of compounds on the expression of apoptosis related proteins (Panel A and B): MDA-MB-231 cells were treated with vehicle or indicated concentrations of compounds for 48 and 72 h. Cells were harvested and lysed for western blot analysis as described in Section 5.1. Blots were probed against apoptosis related proteins (anti-Bax, anti-Bcl-2, anti PARP). Panel C: Annexin binding assay: MCF-7 cells treated 10 μ M of corresponding compounds for 24 h and trypsinized and resuspended in 1 ml of 1 X annexin binding buffer as described in Section 5.1 and subjected to double staining with annexin V-FITC and propidium iodide followed by analysis by flow cytometry.

product. The crude product was purified by column chromatography to yield a pure amorphous sticky solid of **VMY-1-103** (0.070 g, 42%). HRMS ([M+H]) calcd, 708.2847; found, 708.2659.

^1H NMR (400 MHz, CDCl_3): δ 1.00 (dd, 6H, $J = 1.3$ Hz, $J = 6.7$ Hz) 1.44 (dd, 6H) 1.96 (m, 1H) 2.84 (s, 6H), 3.19 (d, 2H, $J = 4.3$ Hz), 3.50 (m, 2H), 3.75 (t, 1H, $J = 9.1$ Hz), 3.99 (m, 2H) 4.43 (bs, 1H), 5.34 (brs, 1H), 5.56 (brs, 1H), 7.10 (t, 2H, $J = 8.0$ Hz), 7.46 (m, 2H), 7.55 (s, 1H), 7.87 (s, 1H), 8.23 (dd, 1H, $J = 1.0$ Hz, $J = 7.3$ Hz), 8.34 (d, 1H, $J = 8.6$ Hz), 8.50 (d, 1H, $J = 8.5$ Hz), 8.57 (s, 1H).

^{13}C NMR (100 MHz, CDCl_3): δ 167.2, 159.4, 151.8, 151.1, 142.1, 135.1, 134.9, 130.8, 130.3, 129.8, 129.7, 129.5, 129.3, 128.2, 127.0, 123.1, 119.9, 118.8, 117.0, 115.1, 114.4, 64.0, 59.3, 53.4, 46.3, 45.3, 42.8, 40.2, 30.2, 22.6, 22.1, 19.3, 19.1.

5.3. Molecular modeling

Docking simulations were carried out using the program SurflexDock within Sybyl 8.2 (Tripos Inc., St. Louis, USA) with the parameters set to default, except the number of ligand conformations generated which was set to 90. After consistent manual intervention of the best selected pose, a final model was obtained. The CDK2/**VMY-1-103** complex structure was then refined by molecular dynamics simulation using the AMBER 9 program suite³⁵ with the PARM98 force-field parameter. The charge and force-field parameters of **VMY-1-103** were obtained using the most recent Antechamber module in the AMBER 9 program, where **VMY-1-103** was minimized at the MP2/6-31G* level. The SHAKE algorithm³⁶ was used to keep all bonds involving hydrogen atoms rigid. Weak coupling temperature and pressure coupling algorithms³⁷ were used to maintain constant temperature and pressure, respectively. Electrostatic interactions were calculated with the Ewald particle mesh method³⁸ with a dielectric constant at $1R_{ij}$ and a nonbonded cutoff of 12 Å for the real part of electrostatic interactions and for van der Waals interactions. The system was then solvated in a 14 Å cubic box of water where the TIP3P model⁸ was used. A 3000 step minimization of the system was performed in which the CDK2 complex was constrained by a force constant of 100 kcal/mol/Å². After minimization, a 5 ps simulation was used to gradually raise the temperature of the system to 298 K while the complex was constrained by a force constant of 20 kcal/mol/Å². Another 10 ps equilibration run was used where only the backbone atoms of the complex were constrained by a force constant of 5 kcal/mol/Å². Final production run of 50 ps was performed with no constraints. When applying constraints, the initial complex structure was used as a reference structure. The PME method was used with a time step of 5 fs. The neighboring pairs list was updated every 30 steps.

5.4. Biological assays

5.4.1. Cell lines and culture

The human breast cell lines MDA-MB-231 (HTB-26) and MCF-7 (HTB-22) were provided by the tissue culture core facility at Lombardi Comprehensive Cancer Center, Georgetown University Medical Center. MCF-7^{MDR} (CL 10.3) cells were gifted by Dr. Robert from the Georgetown University Medical Center. MDA-MB-231, MCF-7, and CL 10.3 cells were maintained at 37 °C in a humidified incubator in DMEM supplemented with heat inactivated fetal bovine serum (10%), 2 mM L-glutamine, and 50 μ g/mL each of antibiotics, namely penicillin, streptomycin, and neomycin.

5.4.2. Cell viability assay (WST-1)

Human breast cancer cells were seeded into a 96-well plate at 3000 cells per well in DMEM containing 10% FBS and allowed to incubate for 24 h. Compounds were dissolved in DMSO, serially diluted in tissue culture media (1–100 μ M), added to cells in triplicate, and incubated for 48 h at 37 °C. Control cells were treated with an equal amount of DMSO. After 48 h of incubation, cell viability was measured by a WST-1 assay according to the manufacturer's instructions (Roche). Briefly, 20 μ L of WST-1 solution was added in each well and incubated for 2–3 h. The water soluble tetrazolium salt of WST-1 is converted into orange formazan by dehydrogenase in the mitochondria of living cells. The formazan absorbance, which correlates to the number of living cells, was measured at 450 nm and 630 nm as reference filter using a microplate reader (Ultramark, Microplate Imaging System, Bio-Rad). The IC₅₀ was calculated from the graph of the log of the compound concentration versus the fraction of the surviving cells.

5.4.3. Cell cycle analysis

The effect of CDK inhibitors on cell cycle progression was analyzed by flow cytometry. Cells were treated with 5 μ M and 10 μ M of **VMY-1-101** or **VMY-1-103** compounds, purvalanol B or roscovitine for 24 h. Cells were trypsinized, centrifuged (2000 rpm), and the cell pellets were collected. Pellets were washed once time with PBS, permeabilized with 70% (v/v) ethanol, resuspended in 1 mL of PBS containing 1 mg/mL RNase and 50 mg/mL propidium iodide, incubated in the dark for 30 min at room temperature, and analysed using a FACSort Flow Cytometer (Becton Dickinson, San Jose, CA). The cell cycle distribution was evaluated on DNA plots using the Modfit software (Verity softwarehouse, Topsham, ME).

5.4.4. Western blot analysis

Western blotting was performed according to literature protocol.³⁹ In brief, cell pellets were collected at the indicated times after treatment with each compound, suspended in 100 μ L of lysis buffer (50 mM Tris–HCl, 150 mM NaCl, 1 mM EGTA, 1 mM EDTA, 20 mM NaF, 100 mM Na₃VO₄, 0.5% NP-40, 1% Triton X-100, 1 mM PMSF, 5 μ g/mL aprotinin, 5 μ g/mL leupeptin), vortexed twice and incubated in an ice bath for 30 min. Lysates were cleared by centrifugation at 12,000 rpm for 15 min at 4 °C and protein content was estimated by detergent compatible BCA protein assay kit (Pierce). Equivalent amounts of total protein were resolved by SDS–PAGE (10%) and transferred to PVDF membrane. Membranes were blocked by 5% non-fat powdered milk in TBST overnight. Membranes were incubated with indicated primary antibodies for 2 h followed by HRP-conjugated secondary antibodies for 1 h and developed using enhanced chemiluminescence kit (Perkin Elmer).

5.4.5. Annexin V binding assay

The loss of phospholipid asymmetry of the plasma membrane is an early event of apoptosis.^{40,41} The annexin V binding assay was performed according to protocol (BD Pharmingen™) to detect this early event of apoptosis. Cells were washed twice with cold PBS and then resuspended in 1 \times binding buffer at a concentration of 1 \times 10⁶ cells/mL. Solution (100 μ L) was transferred to a 5 μ L culture tube and 5 μ L of annexin V-FITC were added followed by 5 μ L of PI. Cells were vortexed gently and incubated for 15 min at rt in the dark. Immediately after adding 400 μ L of 1 \times binding buffer to each tube, cells were analyzed using a FCSort Flow Cytometer (Becton Dickinson, San Jose, CA) and data were analyzed using FCSEXPRESS Denovo software (Los Angeles, CA). Viable cells were FITC–/PI–, apoptotic cells were FITC+/PI–, and necrotic cells were FITC+/PI+.

5.4.6. Staining procedure for human breast tissue

Human breast tissues (Georgetown University Tissue Bank) were subjected to the autoshaker program 7 for de-waxing and re-hydration, followed by epitope retrieval for 20 min at 100 °C in a steamer, and cooled to rt for 24 min. Tissue were blocked in 10% goat-serum, 10 min at rt, exposed to 5% goat-serum for 2 h at rt and washed twice with distilled water. After epitope retrieval was performed, the breast tissues were exposed to 10 μ M of **VMY-1-103** or dansyl ethylenediamine for 1 h at room temperature. The tissues were washed twice with distilled water for 5 min and mounted in aquamount. Images were taken with multiphoton confocal microscopy X63 oil immersion (Zeiss 510LSM/META/NLO live imaging) at excitation 720 nm and imaged with a band path filter of 480–520 nm.

5.4.7. Confocal microscopy

Breast cancer cells were seeded at a density of 5 \times 10⁵ on sterilized microscope slides coated with poly-D-lysine. After 24 h incubation, slides were washed with serum free medium and treated

with 10 μ M of **VMY-1-103** for 1 h. Cells were washed twice with PBS, fixed with 4% formaldehyde in PBS for 15 min at room temperature and washed again with PBS. For nuclear staining, cells were incubated with propidium iodide for 5 min and washed with PBS and mounted on glass slides using Antifade solution. Images were taken with a multiphoton confocal microscope X63 oil immersion (Zeiss510LSM/META/NLO live imaging) at excitation 720 nm and imaged with a band path filter of 480–520 nm.

5.4.8. Kinase assay

VMY-1-101 and **VMY-1-103** were screened for kinase activity at Millipore in Dundee, UK. Briefly, assays were performed with a Biomek 2000 Laboratory Automation Workstation in a 96-well format (Beckman instruments, Palo Alto, CA, USA) for 40 min at ambient temperature in 25 μ L incubations using [γ -³³P]-ATP. In a final reaction volume of 25 μ L, corresponding CDK/cyclin (h) (5–10 mU) was incubated with 8 mM MOPS pH 7.0, 0.2 mM EDTA, 0.1 mg/mL histone H1, 10 mM Mg(OAc)₂, and [γ -³³P]-ATP (specific activity approx. 500 cpm/pmol, concentration as required). The reaction was initiated by the addition of the MgATP mix. After incubation for 40 min at room temperature, the reaction was stopped by the addition of 5 μ L of a 3% phosphoric acid solution. From the reaction, 10 μ L was spotted onto a P30 filtermat and washed three times for 5 min in 75 mM phosphoric acid and once in methanol prior to drying and scintillation counting.

5.5. Test compounds

Roscovitine and purvalanol B were purchased from Sigma (St. Louis, MO), **VMY-1-101** and **VMY-1-103** were prepared as described below. Drugs were dissolved in DMSO, stored at –20 °C, and diluted in serum free medium immediately before use. All experiments were performed in 5% media.

5.6. Statistical analysis

All experiments were repeated three times, and the data expressed as mean \pm standard deviation (SD). Two-tailed student *t* test was used for statistical analysis of the data. A *P* < 0.05 was taken as the level of significance.

6. Disclosure of potential conflicts of interest

A patent application has been filed by Georgetown University on behalf of the inventors that are listed as authors in this article.

Acknowledgements

We thank Dr. Karen Creswell for flow cytometry and Dr. Susette Mueller for microscopy imaging expertise, the core facilities of the Lombardi Comprehensive Cancer Center and the Drug Discovery Program at Georgetown University Medical Center for financial support. We thank Deborah L. Berry for histological staining of the human breast tissue. We thank Dr. Chris Albanese for his valuable scientific discussions.

Supplementary data

Supplementary data associated with this article can be found, in the online version, at doi:10.1016/j.bmc.2011.02.052.

References and notes

1. Nigg, E. A. *Curr. Opin. Cell Biol.* **1993**, *5*, 187.
2. Nigg, E. A. *Bioessays* **1995**, *17*, 471.
3. Senderowicz, A. M. *Oncogene* **2003**, *22*, 6609.

4. Morgan, D. O. *Annu. Rev. Cell Dev. Biol.* **1997**, *13*, 261.
5. Sherr, C. J. *Science* **1996**, *274*, 1672.
6. Harper, J. W.; Elledge, S. J. *Curr. Opin. Genet. Dev.* **1996**, *6*, 56.
7. Shapiro, G. I. *J. Clin. Oncol.* **2006**, *24*, 1770.
8. Vermeulen, K.; Van Bockstaele, D. R.; Berneman, Z. N. *Cell Prolif.* **2003**, *36*, 131.
9. Collins, I.; Garrett, M. D. *Curr. Opin. Pharmacol.* **2005**, *5*, 366.
10. Malumbres, M.; Barbacid, M. *Nat. Rev. Cancer* **2009**, *9*, 153.
11. Wölfel, T.; Hauer, M.; Schneider, J.; Serrano, M.; Wölfel, C.; Klehmann-Hieb, E.; De Plaen, E.; Hankeln, T.; Meyer zum Büschenfelde, K. H.; Beach, D. *Science* **1995**, *26*, 1281.
12. Easton, J.; Wei, T.; Lathi, J. M.; Kidd, V. J. *Cancer Res.* **1998**, *58*, 2624.
13. Malumbres, M.; Barbacid, M. *Nat. Rev. Cancer* **2001**, *1*, 222.
14. Chang, Y. T.; Gray, N. S.; Rosania, G. R.; Sutherlin, D. P.; Kwon, S.; Norman, T. C.; Sarohia, R.; Leost, M.; Meijer, L.; Schultz, P. G. *Chem. Biol.* **1999**, *6*, 361.
15. Gray, N. S.; Wodicka, L.; Thunnissen, A. M.; Norman, T. C.; Kwon, S.; Espinoza, F. H.; Morgan, D. O.; Barnes, G.; LeClerc, S.; Meijer, L.; Kim, S. H.; Lockhart, D. J.; Schultz, P. G. *Science* **1998**, *281*, 533.
16. Senderowicz, A. M.; Sausville, E. A. *J. Natl. Cancer Inst.* **2000**, *92*, 376.
17. Brasca, M. G.; Amboldi, N.; Ballinari, D.; Cameron, A.; Casale, E.; Cervi, G.; Colombo, M.; Colotta, F.; Croci, V.; D'Alessio, R.; Fiorentini, F.; Isacchi, A.; Mercurio, C.; Moretti, W.; Panzeri, A.; Pastori, W.; Pevarello, P.; Quartieri, F.; Roletto, F.; Traquandi, G.; Vianello, P.; Vulpetti, A.; Ciomei, M. *J. Med. Chem.* **2009**, *52*, 5152.
18. Popowycz, F.; Fournet, G.; Schneider, C.; Bettayeb, K.; Ferandin, Y.; Lamigeon, C.; Tirado, O. M.; Mateo-Lozano, S.; Notario, V.; Colas, P.; Bernard, P.; Meijer, L.; Joseph, B. *J. Med. Chem.* **2009**, *52*, 655.
19. Rizzolio, F.; Tuccinardi, T.; Caligiuri, I.; Lucchetti, C.; Giordano, A. *Curr. Drug Targets* **2010**, *11*, 279.
20. Krystof, V.; Uldrijan, S. *Curr. Drug Targets* **2010**, *11*, 291.
21. Davies, T. G.; Pratt, D. J.; Endicott, J. A.; Johnson, L. N.; Noble, M. E. *Pharmacol. Ther.* **2002**, *93*, 125.
22. Knockaert, M.; Greengard, P.; Meijer, L. *Trends Pharmacol. Sci.* **2002**, *23*, 417.
23. Knockaert, M.; Gray, N.; Damiens, E.; Chang, Y. T.; Grellier, P.; Grant, K.; Fergusson, D.; Mottram, J.; Soete, M.; Dubremetz, J. F.; Le, R. K.; Doerig, C.; Schultz, P.; Meijer, L. *Chem. Biol.* **2000**, *7*, 411.
24. Becker, F.; Murthi, K.; Smith, C.; Come, J.; Costa-Roldan, N.; Kaufmann, C.; Hanke, U.; Degenhart, C.; Baumann, S.; Wallner, W.; Huber, A.; Dedier, S.; Dill, S.; Kinsman, D.; Hediger, M.; Bockovich, N.; Meier-Ewert, S.; Kluge, A. F.; Kley, N. *Chem. Biol.* **2004**, *11*, 211.
25. Stearns, M. E.; Jenkins, D. P.; Tew, K. D. *Proc. Natl. Acad. Sci. U.S.A.* **1985**, *82*, 8483.
26. Summerer, D.; Chen, S.; Wu, N.; Deiters, A.; Chin, J. W.; Schultz, P. G. *Proc. Natl. Acad. Sci. U.S.A.* **2006**, *103*, 9785.
27. Damianovich, M.; Ziv, I.; Heyman, S. N.; Rosen, S.; Shina, A.; Kidron, D.; Aloya, T.; Grimberg, H.; Levin, G.; Reshef, A.; Bentolila, A.; Cohen, A.; Shirvan, A. *Eur. J. Nucl. Med. Mol. Imaging* **2006**, *33*, 281.
28. Cohen, A.; Ziv, I.; Aloya, T.; Levin, G.; Kidron, D.; Grimberg, H.; Reshef, A.; Shirvan, A. *Technol. Cancer Res. Treat.* **2007**, *6*, 221.
29. Clarke, R.; Currier, S.; Kaplan, O.; Lovelace, E.; Boulay, V.; Gottesman, M. M.; Dickson, R. B. *J. Natl. Cancer Inst.* **1992**, *84*, 1506.
30. Beck, W. T.; Qian, X. D. *Biochem. Pharmacol.* **1992**, *43*, 89.
31. Meijer, L.; Raymond, E. *Acc. Chem. Res.* **2003**, *36*, 417.
32. Lapenna, S.; Giordano, A. *Nat. Rev. Drug Disc.* **2009**, *8*, 547.
33. Besson, A.; Dowdy, S. F.; Roberts, J. M. *Dev. Cell* **2008**, *14*, 159.
34. Doyle, E. L.; Hunter, C. A.; Phillips, H. C.; Webb, S. J.; Williams, N. H. *J. Am. Chem. Soc.* **2003**, *125*, 4593.
35. Case, D. A.; Darden, T. A.; Cheatham, T. E.; Simmerling, C. L.; Wang, J.; Duke, R. E.; Luo, R.; Merz, K. M.; Pearlman, D. A.; Crowley, M.; Walker, R. C.; Zhang, W.; Wang, B.; Hayik, S.; Roitberg, A.; Seabra, G.; Wong, K. F.; Paesani, F.; Wu, X.; Brozell, S.; Tsui, V.; Gohlke, H.; Yang, L.; Tan, C.; Mongan, J.; Hornak, V.; Cui, G.; Beroza, P.; Matthews, D. H.; Schafmeister, C.; Ross, W. S.; Kollman, P. A. AMBER 9; University of California: San Francisco, 2006.
36. Hanson, R. N.; Lee, C. Y.; Friel, C. J.; Dilis, R.; Hughes, A.; DeSombre, E. R. *J. Med. Chem.* **2003**, *46*, 2865.
37. Berendsen, H. J. C.; Postma, J. P. M.; Vangunsteren, W. F.; Dinola, A.; Haak, J. R. *J. Chem. Phys.* **1984**, *81*, 3684.
38. Darden, T.; York, D.; Pedersen, L. *J. Chem. Phys.* **1993**, *98*, 10089.
39. Deb, T. B.; Coticchia, C. M.; Dickson, R. B. *J. Biol. Chem.* **2004**, *279*, 38903.
40. Fadok, V. A.; Voelker, D. R.; Campbell, P. A.; Cohen, J. J.; Bratton, D. L.; Henson, P. M. *J. Immunol.* **1992**, *148*, 2207.
41. Koopman, G.; Reutelingsperger, C. P.; Kuijten, G. A.; Keehnen, R. M.; Pals, S. T.; van Oers, M. H. *Blood* **1994**, *84*, 1415.
42. Ringer, L.; Sirajuddin, P.; Yenugonda, V. M.; Ghosh, A.; Divito, K.; Trabosh, V.; Patel, Y.; Brophy, A.; Grindrod, S.; Lisanti, M. P.; Rosenthal, D.; Brown, M. L.; Avantaggiati, M. L.; Rodriguez, O.; Albanese, C. *Cancer Biol. Ther.* **2010**, *10*, 326.